Dynamic Surface Tension of Xylem Sap Lipids

Jinlong Yang[1], Joseph Michaud[2], Steven Jansen[3], H. Jochen Schenk[2], and Yi Y. Zuo[1,4*]*

1. Department of Mechanical Engineering, University of Hawaii at Manoa, Honolulu, Hawaii, 96822, USA
2. Department of Biological Science, California State University, Fullerton, California 92831, USA
3. Institute of Systematic Botany and Ecology, Ulm University, Albert-Einstein-Allee 11, D–89081, Ulm, Germany
4. Department of Pediatrics, John A. Burns School of Medicine, University of Hawaii, Honolulu, Hawaii, 96826, USA

Running head: Dynamic surface tension of xylem sap lipids

***Corresponding authors:**
E-mail: jschenk@fullerton.edu (H. Jochen Schenk)

E-mail: yzuo@hawaii.edu (Yi Y. Zuo)

Accepted for publication in Tree Physiology 20 January 2020.

DOI: 10.1093/treephys/tpaa006

Abstract

The surface tension of xylem sap has been traditionally assumed to be close to that of the pure water because decreasing surface tension is thought to increase vulnerability to air seeding and embolism. However, xylem sap contains insoluble lipid-based surfactants, which also coat vessel and pit membrane surfaces, where gas bubbles can enter xylem under negative pressure in the process known as air seeding. Because of the insolubility of amphiphilic lipids, the surface tension influencing air seeding in pit pores is not the equilibrium surface tension of extracted bulk sap, but the local surface tension at gas-liquid interfaces, which depends dynamically on the local concentration of lipids per surface area. To estimate dynamic surface tension in lipid layers that line surfaces in the xylem apoplast, we studied the time-dependent and surface area-regulated surface tensions of apoplastic lipids extracted from xylem sap of four woody angiosperm plants using constrained drop surfactometry. Xylem lipids were found to demonstrate potent surface activity, with surface tensions reaching an equilibrium at about 25 mN / m and varying between a minimum of 19 mN / m and a maximum of 68 mN / m when changing the surface area between 50% and 160% around the equilibrium surface area. It is concluded that xylem lipid films in natural conditions most likely range from nonequilibrium metastable conditions of a supersaturated compression state to an undersaturated expansion state, depending on the local surface areas of gas-liquid interfaces. Together with findings that maximum pore constrictions in angiosperm pit membranes are much smaller than previously assumed, low dynamic surface tension in xylem turns out to be entirely compatible with the cohesion-tension and air-seeding theories, as well as with the existence of lipid-coated nanobubbles in xylem sap, and with the range of vulnerabilities to embolism observed in plants.

Keywords: xylem surfactant, apoplastic xylem lipids, xylem sap, dynamic surface tension, embolism, constrained drop surfactometry, phospholipids, galactolipids, DGDG, MGDG

Introduction

Vascular plants are the only organisms that transport water by taking advantage of cohesion between water molecules to pull it through a hydraulic system rather than pushing it under positive pressure. Pulling stretches the distance between water molecules slightly and thereby creates negative pressure in the water. The pull is caused by evaporation of water from nanocapillaries in the cell walls of leaves (Askenasy 1895; Dixon 1914b; Dixon and Joly 1895), and the negative pressure is generated by the weight of the water column and the hydraulic resistance in the hydraulic system (Hacke et al. 2006; Lucas et al. 2013). Outside vascular plants, negative pressure in aqueous solutions also exists in other systems that possess nanocapillaries from which water evaporates, such as soils and rocks (Graham et al. 1997; Or and Tuller 2002), and such conditions have also been created in engineered devices that are often referred to as synthetic trees (Duan et al. 2012; Thut 1928; Vincent et al. 2012; Wheeler and Stroock 2008). All such systems encompass multiple phases and surfaces between them, including rigid solid walls that do not collapse under the negative pressure, a continuous aqueous phase, solid-liquid surfaces, gas bubbles, and gas-liquid menisci in nanocapillaries. There has been surprisingly little research into surface phenomena in negative pressure systems, except for studies on heterogeneous bubble nucleation at solid surfaces that are in touch with the liquid under negative pressure (Chen et al. 2016; Menzl et al. 2016; Wheeler and Stroock 2009). Understanding the behavior of surfaces under negative pressure is complicated further by the presence of surface-active molecules (surfactants) in the system (Atchley 1989; Schenk et al. 2015; Yount et al. 1977).

The hydraulic system of a vascular plant encompasses the entire plant, but the negative pressure is restricted to the parts outside living cells, including cell walls, intercellular spaces, and the dead cells of the xylem, including vessels and tracheids. Together, these non-living parts are referred to as the apoplast. Surfactants in xylem sap were first documented by Christensen-Dalsgaard et al. (2011) and were found to include amphiphilic lipids, including phospholipids, and proteins (Gonorazky et al. 2012; Schenk et al. 2018; Schenk et al. 2017). A recent lipidomic

77 analysis of lipids extracted from xylem sap found phospholipids (25-93%) and galactolipids (7-
78 75%) (see Table 1), with total lipid concentrations ranging from 0.18 to 0.63 μmol / L of xylem
79 sap (Schenk et al. 2019).

80 Xylem lipids are concentrated on the surfaces of xylem conduits and on the cellulosic and
81 nanoporous pit membranes serving as connections between conduits (Figure 1). Since the three
82 dimensional structure of pit membrane pores is characterized by various pore constrictions, which
83 are typically below 20 nm in diameter, (Choat et al. 2003; Zhang et al. 2019; Zhang et al. 2017),
84 these pit membranes prevent the entry of large gas bubble into water-filled conduits that are under
85 negative pressure (Schenk et al. 2015; Zimmermann 1983). However, surface-active molecules
86 associated with pit membranes would decrease surface tension and thereby increase the likelihood
87 of gas entry through this porous medium (Cochard et al. 2009; Domec 2011; Losso et al. 2017;
88 Schenk et al. 2018; Schenk et al. 2017; Schenk et al. 2019; Schenk et al. 2015). To date, only
89 limited data are available to indicate what the effects of natural xylem surfactants on surface
90 tension in xylem may be (Christensen-Dalsgaard et al. 2011; Losso et al. 2017; Schenk et al. 2017).

91 The behavior of lipid coatings in xylem under fluctuating negative pressure remains subject to
92 speculation until more is known about their surface tension properties. Amphiphilic lipids
93 aggregate on surfaces and are essentially insoluble in water, with very low critical micelle
94 concentrations (CMC; Marsh and King 1986). Thus, surface tension imparted by these lipids
95 depends strongly on their local concentration at a surface, i.e., the surface density of lipid
96 molecules, which may change over time, a phenomenon known as dynamic surface tension (Figure
97 2). Even at very low concentrations in xylem, amphiphilic lipids would minimize their free energy
98 by quickly accumulating on gas-liquid surfaces (Gibbs 1906; Rice 1926) and imparting a surface
99 tension that depends on concentration of lipids per interfacial area and not on the overall lipid
100 concentration per water volume (Figure 2). This dynamic surface tension concept is very different
101 from the surface tension imparted by soluble surfactants in water, such as Tween, Triton-X, or
102 alcohols, which below their CMCs depends on the concentration per volume of water and is
103 essentially constant above CMC. Soluble surfactants have been used experimentally to test for

104 effects of lowering surface tension in xylem (Cochard et al. 2009; Hölttä et al. 2012; Losso et al.
105 2017; Sperry and Tyree 1988).

106 It is impractical to collect lipids directly from coatings on xylem surfaces, but fortunately they
107 are also found in low concentrations in xylem sap. Here, we report research on the dynamic surface
108 tension properties of lipids extracted from xylem sap of four woody angiosperm species measured
109 using constrained drop surfactometry (CDS). The CDS is a novel droplet-based surface
110 tensiometry technology developed in the Zuo laboratory (Figure 3) for studying the surface activity
111 of pulmonary surfactants (Valle et al. 2015). Using CDS, we directly measured the time-dependent
112 and surface area-regulated dynamic surface tensions of lipids extracted from xylem sap, which
113 cannot be measured using standard methods such as the pendant drop technique. The technique
114 was used previously for studying dynamic surface tension of freeze-dried xylem sap extract
115 (Schenk et al. 2017), i.e., non-purified mixtures of proteins, amino acids, carbohydrates, lipids,
116 and salts. In addition, using a newly developed *in situ* Langmuir- Blodgett (LB) transfer technique
117 (Yang et al. 2018), we revealed the ultrastructure of natural xylem lipid films using atomic force
118 microscopy (AFM).

119 We hypothesized that purified xylem sap lipid films would show similar dynamic surface
120 tension to what is found in other natural lipid mixtures, such as pulmonary surfactants (Parra and
121 Pérez-Gil 2015; Zuo et al. 2008), with nonconstant but surface area-regulated dynamic surface
122 tension upon film compression and expansion (Schürch et al. 2010). Galactolipids in xylem lipid
123 mixtures may affect the behavior of films especially at low surface tension, because their galactose
124 headgroups strongly interact with each other, promoting lipid stacking and layering (Bottier et al.
125 2007; Kanduč et al. 2017; Lee 2000). Together with the xylem sap lipidomics analysis in a
126 companion study (Schenk et al. 2019), our data provide a novel insight into the understanding of
127 surface phenomena in xylem of vascular plants and their potential impacts on hydraulic function
128 at the organ to whole-plant level.
129

Materials and Methods

Extraction of xylem lipids

Natural xylem lipids were extracted from xylem sap of four woody plant species, *Distictis buccinatoria* (DC.) A.H.Gentry (syn. *Amphilophium buccinatorium* (DC.) L.G.Lohmann, evergreen vine, Bignoniaceae), *Encelia farinosa* A.Gray ex Torr. (semi-deciduous desert shrub, Asteraceae), *Geijera parviflora* Lindl. (evergreen tree, Rutaceae), and *Liriodendron tulipifera* L. (deciduous tree, Magnoliaceae). These species represent different plant growth forms from four major clades distributed across the angiosperm phylogeny. Stems for xylem sap extraction were collected in August 2017. Because lipid concentrations in sap are very low, as lipids are mostly attached to xylem surfaces, samples (from two stems for *Encelia* and four stems for *Distictis, Geijera*, and *Liriodendron*) were combined into one composite sample per species to ensure a sufficiently high concentration of lipids per sample for surface tension analysis and to create the same lipid composition as in other subsamples analyzed via mass spectrometry (Schenk et al. 2019). Analysis of composite samples does not allow statistical comparisons between species, but such comparisons were not the goal of this study.

Most collections were done at dawn to ensure full hydration of the stems. The extraction protocol was described in detail in Schenk et al. (2019). Branches were cut from the plants at a length exceeding the longest vessel for each species, transported immediately to the lab, and cut under water, with the final cuts made with a fresh razor blade. The bark was removed from the proximal end for about 4 cm length to expose the xylem cylinder and to avoid phloem contamination. The cut surface was thoroughly cleaned with deionized water using a high-pressure dental flosser (WP-100 Ultra Water Flosser, Waterpik Inc., Fort Collins, CO, USA) for two minutes to remove cell debris and cytoplasmic content from the surface. Xylem sap was extracted from the proximal end of the stem under vacuum into a glass test tube embedded in ice inside a 1 L Buchner flask. The flask was subjected to lab vacuum for about 30 seconds, after which the distal end of the branch was cut back by about 4 cm, followed by successive 2 cm cuts made to all the side branches until sap was observed dripping into the test tube. Further 1 cm cuts were made every minute to allow

for slow, continuous extraction of xylem sap. Depending on stem size, 1 to 2 mL of sap were extracted from each stem, moved in a glass pipette into pre-weighed 1.5 mL LoBind Eppendorf microcentrifuge tubes, flash-frozen in liquid nitrogen and stored in the freezer until further processing.

Samples were also taken to test for contamination of sap samples by lipids from living cell remnants (Schenk et al. 2017). This was done prior to xylem sap extraction by inserting the cleaned, cut ends of xylem into a glass vial containing 1 mL of nanopure water. Lipid concentrations in these controls for the four study species ranged from 1.1 to 6.7% of the lipids found in xylem sap (Schenk et al. 2019), which was too low to be included in surface tension measurements. Other tests have shown that xylem sap lipids are not contaminants that originate from repeated cuts of stems made during the vacuum extraction (Schenk et al. 2019) and the ordered nature of lipid layers observed on xylem surfaces (Figure 1) (Schenk et al. 2018; Schenk et al. 2017) also rules out contamination as the source of xylem sap lipids.

Xylem sap samples in LoBind Eppendorf microcentrifuge tubes were partially lyophilized in a freeze-dryer (FreeZone 1 Liter Benchtop Freeze Dry System, Labconco, Kansas City, MO, USA) until only about 100 μL of sample remained in each tube. The remaining aqueous samples were combined into one sample for each species using a glass pipette and weighed. Methanol:chloroform 1:1 (both HPLC grade, Fisher Scientific) was added to the combined aqueous sample to create an approximate 5:5:1 methanol:chloroform:water one-phase mixture. The mixture was then vortexed, centrifuged, and the supernatant was collected using a 1 mL glass syringe with PrecisionGlide Needle. A new one-phase 5:5:1 mixture of methanol:chloroform:water was then added to the residue, the mixture vortexed, centrifuged, and the supernatant again was collected and combined with the previously collected supernatant. Samples were dried in a desiccator outfitted with an in-line carbon filter capsule (model 6704-7500, Whatman, GE Healthcare Life Sciences, UK) and sent to the Zuo lab at the University of Hawaii at Manoa for analysis. Other samples from these same collections and extracted the same

183 way were sent out for mass spectrometry analyses to determine the lipid compositions, which are
184 reported in a separate paper (Schenk et al. 2019).
185 Xylem lipids extracted via this protocol also include very low concentrations of hydrophobic
186 proteins determined by Tris-Tricine-SDS-PAGE to be between 5 and 18 kDa in size (data not
187 shown). The very low concentrations have prevented the identification of these proteins to date.
188 ***Constrained drop surfactometry (CDS)***
189 Dynamic surface tension measurements and surfactant film imaging were carried out with
190 constrained drop surfactometry (CDS) (Valle et al. 2015). CDS is a new generation of drop-based
191 surfactometer. As shown in Figure 3, it uses a sessile drop (~3 mm in diameter) to generate the
192 air-water surface, where the natural surfactant sample is spread and studied. The sessile drop is
193 confined on a carefully machined pedestal that uses a knife-sharp edge to prevent the droplet from
194 spreading at low surface tensions. The spread surfactant film can be compressed and expanded by
195 withdrawing and injecting liquid into the droplet using a motorized syringe. Surface tension is
196 determined photographically from the shape of the droplet using axisymmetric drop shape analysis
197 (ADSA) (Yang et al. 2017).
198 For CDS measurement, each freeze-dried xylem lipid sample was dissolved in 50 μL of
199 chloroform. The samples were subjected to 5 minutes of ultrasonic treatment, followed by 1 minute
200 of vortex treatment to create a homogeneous solution, after which 1 μL of xylem lipid sample was
201 spread at the surface of the pure water droplet (Milli-Q ultrapure water; Millipore, Billerica, MA)
202 of the CDS instrument, where it was left undisturbed for 1 min to allow film spreading and
203 evaporation of the chloroform. Time-dependent dynamic surface tension was recorded with ADSA
204 until an equilibrium surface tension (γ_e) was reached. Subsequently, the xylem surfactant film was
205 compressed and expanded at a rate of 0.1 cm^2/min. The surface area-regulated surface tension was
206 recorded during three compression-expansion cycles for each composite sample. All
207 measurements were conducted at room temperature of 20 ± 1°C.

208 ***Film imaging with atomic force microscopy (AFM)***

209 To determine if the lipid films were smooth monolayers at γ_e, the molecular organization and
210 lateral structure of the spread xylem lipid films at γ_e was visualized via AFM. The films were
211 Langmuir-Blodgett (LB) transferred from the air-water surface to a small piece of freshly peeled
212 mica sheet by lifting the mica through the drop surface at a rate of 1 mm / min as described in
213 Yang et al. (2018). Topographical images of the xylem lipid films were obtained using an Innova
214 AFM (Bruker, Santa Barbara, CA). Samples were scanned in air in contact mode using a silicon
215 nitride cantilever with a spring constant of 0.12 N / m and a tip radius of 2 nm. Lateral structures
216 were analyzed using Nanoscope Analysis (version 1.5).

217

218 **Results**

219 ***Time-dependent dynamic surface tension of xylem lipids***

220 Figure 4 shows the time-dependent dynamic surface tensions of xylem lipids extracted from
221 *Distictis buccinatoria, Encelia farinosa, Geijera parviflora,* and *Liriodendron tulipifera*.
222 Reproducibility of these dynamic surface tension measurements within each composite sample can
223 be found in Figure S1 of the Supporting Information (SI). After spreading at the air-water surface,
224 the xylem lipids immediately reduced surface tension below 40 mN / m. They further reduced the
225 surface tension to an equilibrium value (γ_e) around 25 mN / m within 2-3 seconds. The γ_e for xylem
226 lipids of all four species are very close and are consistent with that of the adsorbed film from fully-
227 hydrated phospholipids bilayers (Zuo et al. 2008).

228 ***Surface area-regulated surface tension of xylem lipids***

229 Figure 5 shows the surface area-regulated dynamic surface tension of the xylem lipids for the four
230 plant species. Reproducibility of these compression-expansion cycles within composite samples
231 can be found in Figure S2 of the SI. In these experiments, the equilibrium xylem surfactant films
232 at γ_e were first compressed to approximately 60% of the original area and subsequently expanded
233 to 160% of the original area. When an insoluble surfactant film at equilibrium is compressed, it
234 enters a metastable compression regime. All four xylem lipid films were remarkably similar

between species, despite the differences in lipid composition (Table 1). Lipid films quickly reach a minimum surface tension (γ_{min}) around 19 mN / m when the films are compressed by less than 5% of the original area. This γ_{min} is in line with the collapse surface tension reported for the two galactolipids in xylem lipid, MGDG and DGDG (Gzyl-Malcher et al. 2008; Hoyo et al. 2016). The γ_{min} does not change significantly with further area reduction by 40% of the lipid film. Upon expansion, all four xylem lipid films show an abrupt surface tension increase to γ_e, i.e., around 25 mN / m. The surface tension is stabilized at γ_e until the film is expanded beyond its original surface area. With further expansion, the lipid film enters a metastable expansion regime, in which the surface tension increases continuously with area expansion to 160% of its original area. The film is then compressed again with decreasing surface tension to complete a cycle.

Ultrastructure of xylem lipid films

Figure 6 shows the AFM topographic images of the four xylem lipid films at the equilibrium surface tension (γ_e). Reproducibility of these AFM topographic images within composite samples can be found in Figure S3 of the SI. At γ_e, the lipid film at the air-water surface reaches a dynamic equilibrium with lipid micelles and vesicles in the subphase. As shown in Figure 6, all xylem lipid films maintain a lateral structure of coexisting interfacial monolayer with randomly distributed protrusions. Although the thickness of the background layer is unknown, its smoothness shows it to be a monolayer, as lipids prone to multilayer formation would form a much bumpier surface. Height analysis indicates that the sizes of most protrusions are multiples of 4 nm, which is the thickness of a fully hydrated lipid bilayer (Nagle and Tristram-Nagle 2000). Hence, these protrusions most likely represent multilayers of lipids attached to the interfacial monolayer of the xylem surfactant under the equilibrium condition. The number and height of the protrusions are different for the xylem lipid from the four plant species. Lipids from *Distictis* and *Liriodendron*, which have the largest amounts of galactolipids (Table 1), have the fewest peaks, and most are around 8 nm in height. Although the number of 8 nm peaks is highest in *Distictis* and *Liriodendron*, a 12 nm peak was found for *Encelia*. These images support the conclusion that xylem lipids form

monolayers at equilibrium surface tension but begin to create folds and stacks that are likely to increase upon further compression of the layer.

Discussion

An aqueous liquid under negative pressure is in a metastable state and is prevented from turning into vapor by the nucleation energy required to break hydrogen bonds between water molecules and form a void (Chen et al. 2016; Menzl et al. 2016; Wheeler and Stroock 2009). Pure water has very high tensile strength, up to a theoretical maximum of -190 MPa or at least to an experimentally achievable maximum of -30 MPa (Caupin et al. 2012), which prevents homogeneous nucleation under negative pressure in plants (Oertli 1971; Stroock et al. 2014). Xylem sap, however, is not pure water, and the presence of salts, organic solutes, and especially surface-active molecules, would affect nucleation thresholds (Dixon 1914b; Hemmingsen 1978). Because of the perception that low surface tension would increase vulnerability to embolism, the surface tension of xylem sap has been traditionally assumed to be equal to that of the pure water (Meyra et al. 2007; Oertli 1971; Tyree and Zimmermann 2002). That assumption, however, has proved to be incorrect (Christensen-Dalsgaard et al. 2011; Domec 2011; Losso et al. 2017; Schenk et al. 2017). Moreover, the functional significance of surface-active insoluble lipids on xylem surfaces demands the consideration of not just the equilibrium surface tension of bulk xylem sap, but the concentration-dependent, local surface tension at phase interfaces in xylem.

Here, we determined both time-dependent and surface area-regulated dynamic surface tensions of natural lipids extracted from xylem sap. It was found that when spread at the air-water surface, all xylem lipids quickly reach an equilibrium (γ_e) by reducing the surface tension of the air-water surface from 72 mN / m to about 25 mN / m within a few seconds (Figure 3), indicating a potent surface activity. When compressed below γ_e, the xylem lipid films maintain a supersaturated metastable state without collapse and reduce the surface tension to a minimum surface tension (γ_{min}) around 19 mN / m. Presumably further compression could further reduce the surface tension towards zero, as the lipid layers stack and fold. When expanded above γ_e, the xylem surfactant

288 films maintain an undersaturated metastable state and increase the surface tension to a maximum
289 (γ_{max}) of 52 mN / m for *Encelia farinosa* and 68 mN / m for *Distictis buccinatoria*, i.e., closer to
290 the surface tension of pure water (Figure 5). The shapes of surface tension curves as function of
291 drop surface area are remarkably similar between species (Figure 5), despite considerable
292 differences in lipid composition (Table 1).

293 Our hypothesis that xylem lipids would show similar dynamic surface tension to other
294 biological lipid mixtures, such as pulmonary surfactants, was supported by these findings.
295 Dynamic changes in surface tension are crucial for the function of alveoli in lungs (Parra and
296 Pérez-Gil 2015), but it remains to be investigated what their functional importance is in the
297 angiosperm xylem, where changes in pressure that affect gas-liquid interfaces typically show
298 diurnal and seasonal fluctuations, not many fluctuations per minute, as in lungs. Effects of
299 compression and expansion rates on dynamic surface tension (see Fig. S2 in Supporting
300 Information) merit further investigation, as not all pressure changes in plants are slow. Embolism
301 formation in a xylem conduit creates a sudden, local pressure increase (Hölttä et al. 2009), and it
302 remains to be investigated how lipid layers on air-water interfaces would respond to such an
303 extremely rapid change in surface conditions.

304 The presence of substantial amounts of galactolipids in xylem sap (6.9% in *Encelia* to 34.4%
305 in *Liriodendron*; Table 1) was very unexpected, as both are plastid lipids, and MGDG has never
306 been found outside of plastids before (Dörmann and Benning 2002; Kalisch et al. 2016).
307 Apoplastic galactolipids in xylem vessels most likely originate from the original cell content of
308 the living vessels before programmed cell death, although this requires further research (Esau
309 1965; Esau et al. 1966; Schenk et al. 2019). The role of galactolipids in the dynamic surface tension
310 patterns shown in Figs. 4 and 5 requires further investigation. Galactolipids are typically highly
311 unsaturated (Dörmann and Benning 2002; Kalisch et al. 2016), and unsaturated MGDG, which
312 made up between 4.0 and 26.6% of all xylem lipids in this study, do not form bilayers by
313 themselves, because their small headgroup and spreading acyl chains give them a cone-shape that
314 favors curved shapes of lipid layers (Lee 2000). However, strong head-group interactions between

galactolipids favor stacking, such as seen in the grana of thylakoids in chloroplasts (Bottier et al. 2007; Kanduč et al. 2017; Lee 2000; Simidjiev et al. 2000). Galactolipids may be especially prone to stacking and folding and could be responsible for the distinct inward folding of lipid coats seen in freeze-fracture electron micrographs of lipid-coated nanobubbles from xylem sap in Fig. 8C in Schenk et al. (2017) and the multilayered structures seen under AFM, even at equilibrium surface tension, γ_e (Figure 6).

Most xylem sap lipids are phospholipids, especially phosphatidic acid (PA) and phosphatidylcholine (PC) (Table 1), and the composition of phospholipid headgroups is likely to affect some of the differences in dynamic surface tension between species. For example, the headgroup of PA is small and negatively charged, with a tendency toward forming nanodomains and concave (inward) curvature of lipid layers (Kooijman et al. 2003). However, surface tension is more strongly affected by acyl chain characteristics, and these were very similar between species, with about 84% of acyl chain lengths of 17 and 18 carbon atoms, >98% unsaturated, and with mostly 1-3 double bonds for chain lengths of 17 and 3-5 double-bonds for chain lengths of 18. The similarity in chain lengths and degree of saturation could explain why minimum and equilibrium surface tension was remarkably similar between species. Further research will be required to determine the effects of lipid composition on the differences in surface tension between species, including their effects on folding, stacking and formation of nanodomains by phase separation, best studied via AFM at minimum and maximum surface tension.

Comparison to previous surface tension measurements of xylem sap

Both γ_e and γ_{min} determined here are significantly lower than the traditionally estimated and measured surface tension of bulk xylem sap (Christensen-Dalsgaard et al. 2011; Losso et al. 2017; Tyree and Zimmermann 2002). A previous study of the surface tension of xylem sap of three angiosperm tree species using the pendent drop method (Christensen-Dalsgaard et al. 2011) found that given a long-enough time (i.e., 30 min), the surface tension of xylem sap can be reduced to the range of 52-58 mN / m, most likely caused by a reduction of surface area due to evaporation from the drop, which was not in a vapor-saturated environment. In a later study, the surface tension

342 of xylem sap extracted from two conifers was measured using the sessile drop method (Losso et
343 al. 2017), finding that the equilibrium surface tension showed seasonal variations and fluctuated
344 between 50 and 68 mN / m over the year. Minimum surface tensions reported by these researchers
345 are closer to the maximum surface tension (γ_{max}) determined in the present study.
346 The differences between the present study and previous measurements can be explained by the
347 following two facts. First, both previous measurements (Christensen-Dalsgaard et al. 2011; Losso
348 et al. 2017) did not study the surface area-regulated, dynamic surface tension. Second, both
349 previous measurements (Christensen-Dalsgaard et al. 2011; Losso et al. 2017) used extracted
350 xylem sap without further purification and concentration. In contrast, the xylem lipids studied here
351 are purified (by organic solvent extraction) and concentrated (by pooling multiple xylem sap
352 samples). Consequently, the xylem lipids studied here show significantly more potent surface
353 activity than the xylem sap studied before, as indicated by a much faster adsorption (reaching
354 equilibrium within 5 seconds vs. >30 min) and a much lower γ_e (25 mN / m vs. >50 mN / m). A
355 look at the xylem conduits shown in Figure 1 (also see Schenk et al. 2018) demonstrates why it
356 makes sense to measure surface tension of lipid films rather than that of extracted xylem sap. Lipid
357 layers on inner vessel wall surfaces and in bordered pits create high local lipid concentrations at
358 locations where bubble nucleation is most likely to occur, while most of the surface-attached lipids
359 are unlikely to appear in extracted and non-purified xylem sap. Therefore, the equilibrium surface
360 tension measurements of extracted bulk xylem sap do not provide any information about the
361 functional significance of surfactants in water conducting cells of xylem tissue. On the other hand,
362 while lipid extraction from sap is necessary to concentrate the lipids for realistic surface tension
363 measurements, extraction removes other components found in sap, such as ions, proteins, and
364 carbohydrates, that may interact with lipids in xylem. Future research will have to compare the
365 behavior of lipids in the presence and absence of these other xylem components.
366 Our data therefore indicate that the xylem surfactant films studied previously were most likely
367 at an undersaturated expansion state, as they were conducted with xylem sap with very low
368 surfactant concentrations (Schenk et al. 2017; Schenk et al. 2019), and using static drop-based

methods that did not include drop compression (Christensen-Dalsgaard et al. 2011; Losso et al. 2017), except for potential evaporation from a pendant drop, potentially causing it to shrink and decreasing surface tension (Christensen-Dalsgaard et al. 2011). The droplet for surface tension measurements usually has a diameter of 3-4 mm, corresponding to a surface area of 0.15 to 0.4 cm^2 (Figure S2). This drop size is required by the measurement principle of drop shape analysis. When the drop/bubble is smaller than the capillary length (e.g., 2.7 mm for pure water), it cannot be effectively deformed by gravity and thus maintains a nearly-spherical shape that fails the surface tension measurements from shape analysis (Yang et al. 2017). The difference between our study and previous ones is not in the size of the droplet, but in the changing concentration of surface-active molecules on the droplet's surface, which is needed to understand the concentration-dependent local surface tension.

Implications of dynamic surface tension of lipids for xylem function

Dynamic surface tension commonly shows hysteresis between compression and expansion (Figure 5) (Ingenito et al. 1999; Zuo et al. 2008), due to processes such the formation, dissolution, and tearing of lipid domains (Kwan and Borden 2010), lipid layer folding during compression and unfolding during expansion, and replenishment of lipids from micelles into stretched lipid films (Figure 2). Hysteresis may be important in the face of pressure-fluctuations in xylem conduits. Xylem commonly experiences diurnal fluctuations in negative pressure that can exceed 2 MPa (Meinzer et al. 2016), with the most negative pressures occurring in the middle of the day and less negative ones often just before dawn. Large fluctuations in pressure would affect phase interfaces in xylem and cause area variations of the lipid-covered surface, thus actively regulating the surface tension. Hysteresis effects are most likely short-lived, as lipids can migrate quickly between micelles in bulk and phase interfaces, but hysteresis phenomena in lipid films could play an important role in response to sudden pressure fluctuations, such as a sudden local tension-relief caused by the formation of an embolism (Hölttä et al. 2009).

The most likely sources for emboli in xylem are pores in pit membranes between sap-filled and gas-filled conduits (Hacke and Sperry 2001; Jansen and Schenk 2015; Meyra et al. 2007;

Zimmermann 1983). Estimated pore constrictions in fresh (fully hydrated, non-dried) pit membranes of angiosperms are much smaller (<20 nm in diameter) than previously assumed, while previous estimates of maximum pore sizes were based on a simplistic, two dimensional view of pores, and affected by drying artifacts (Zhang et al. 2019; Zhang et al. 2017). According to the Young Laplace equation, the pressure difference required to force a bubble through a 20 nm pore, assuming a contact angle of zero (Caupin et al. 2008; Meyra et al. 2007), and a pore shape correction factor for non-cylindrical pores of 0.5 (Schenk et al. 2015), would be 7.2 MPa in pure water. Most angiosperms are vulnerable to air seeding far below that value (Choat et al. 2012). With lipids in pit membrane pores, if the surface tension of an air-water meniscus is reduced to 25 mN / m, the equilibrium surface tension found in this study, a meniscus could pass through a 20 nm pore with a shape correction factor of 0.5 under a pressure difference of 2.5 MPa. This is a far more realistic value for air seeding to cause embolism in angiosperms than 7.2 MPa (Choat et al. 2012).

The assumption that a rare pit membrane with a much larger pore will trigger embolism formation at a similar air-seeding pressure is frequently suggested in literature (Plavcová et al. 2013; Wheeler et al. 2005). This hypothesis, however, does not consider the presence of xylem sap surfactants and the three dimensional structure of the pit membrane pore space, which consists of various pore constrictions with highly variable pore volumes, depending on the overall pit membrane thickness and the number of cellulose microfibril layers (Jansen et al. 2018; Kaack et al. 2019; Zhang et al. 2019). Low surface tension in xylem is therefore entirely compatible with the cohesion-tension and air-seeding theories and with the range of observed vulnerabilities to embolism in plants, while xylem sap with the high surface tension of pure water is incompatible with both the theories and observations.

Xylem lipids not only coat solid surfaces but have also been found to coat nanobubbles in extracted xylem sap (Schenk et al. 2017). It is impossible to know for certain if lipid-coated nanobubbles exist in sap that is under negative pressure in intact xylem, but their existence in aqueous solution under fluctuating negative pressure is theoretically possible if their surface

tensions were sufficiently low (Atchley 1989; Schenk et al. 2017; Schenk et al. 2015). In fact, closely packed insoluble surfactant monolayers and the resultant regulation of surface tension due to surface area variations may be the only way to allow very small gas bubbles to exist in a liquid (Atchley 1989; Yount 1979; Yount 1997; Yount et al. 1977). Otherwise, a small gas bubble in water would either dissolve instantaneously because of the excess Laplace pressure inside the bubble, or expand into an embolism if the differences between the sap pressure and the internal gas pressure in the bubble exceeded the pressure originating from the surface tension (Atchley 1989; Schenk et al. 2017). Lipid-coated nanobubbles could originate from liquid-lipid-gas interfaces moving through highly variable pore volumes with multiple pore constrictions. The resulting nanobubbles need to be smaller than the critical size that causes bubble expansion depending on surface tension (Schenk et al. 2017). Bubbles larger than that critical size would expand and either continue to be stabilized by increasing area-dependent surface tension (Figure 2, 5) or continue expanding to form a xylem embolism.

Obviously, xylem in a living plant experiences constant changes in temperature, pressure, and dissolved gas concentrations (Schenk et al. 2016), and simple equilibrium models cannot do justice to ever-changing conditions. The dynamic surface tension data presented in this study will allow the development of more realistic dynamic models to predict the formation and behavior of lipid-coated nanobubbles and of other phase interfaces in xylem, especially at pit membranes.

Remarkably, the first one to suggest a role of colloids for enabling water transport under negative pressure in plants was no other than Henry Dixon, one of the originators of the cohesion-tension theory (Dixon 1914a, b). The evidence presented in this study sheds novel light on the longstanding question of how plants transport water under negative pressure, which remains incompletely understood, especially with respect to the mechanism(s) that prevent embolism formation and the temporal frequency of hydraulic failure.

Conclusions

Contrary to long-standing assumptions, the apoplast of angiosperm xylem contains amphiphilic lipids, which are insoluble and accumulate on surfaces, including at air-water interfaces. Using constrained drop surfactometry, we were able to study the time-dependent and surface area-regulated dynamic surface tensions of apoplastic lipids. These were extracted from xylem sap, because it is impractical to collect lipids directly from surfaces in the xylem. It is found that xylem lipids extracted from all four tree species demonstrate potent surface activity. Surface tensions of the xylem surfactants reach an equilibrium at 25 mN / m and vary between a minimum value of 19 mN / m and a maximum value of 68 mN / m when changing the surface area between 60% and 160% around the surface area at equilibrium. We therefore concluded that xylem lipid films in natural conditions vary most likely between nonequilibrium conditions of a supersaturated metastable compression state and an undersaturated metastable expansion state, depending on the local surface area available at phase interfaces, which could be affected by changes in liquid pressure. Open questions to be addressed in future research include the exact origin of xylem sap lipids, the behavior of surfactant coated air-water-solid interfaces under negative pressure, effects of other types of molecules on the dynamic surface tension of lipid films in xylem, and how exactly air-seeding would work based on a dynamic surface tension concept. Our study provides a novel understanding of how xylem lipids both affect air seeding through the tiny pore constrictions of angiosperm pit membranes, and can also stabilize resulting nanobubbles, thus collectively reducing the vulnerability to embolism at the organ and whole-plant level.

Acknowledgements

The authors thank Tatiana Melendres for assistance with xylem sap extractions, Greg Pongetti at the Fullerton Arboretum for allowing sampling of plants, and Aissa Do and Alison Miyamoto for conducting protein analyses of xylem lipid mixtures.

Conflict of interest

We declare that we have no conflict of interest.

Funding

The research was funded by the National Science Foundation IOS-1558108 and IOS-1754850 (H.J.S., S.J., and Y.Y.Z.) and CBET-1604119 (Y.Y.Z.). S.J. acknowledges funding from the German Research Foundation (Individual Research Grant No. 383393940).

Supporting Information

Reproducibility of the surface tension measurements, compression of the film at two compression rates, and AFM imaging.

References

Askenasy, E. 1895. Ueber das Saftsteigen. Verhandlungen des Naturhistorisch-medizinischen Vereins zu Heidelberg, N.F. 5:325-345.

Atchley, A.A. 1989. The Blake threshold of a cavitation nucleus having a radius‐dependent surface tension. The Journal of the Acoustical Society of America. 85:152-157.

Bottier, C., J. Géan, F. Artzner, B. Desbat, M. Pézolet, A. Renault, D. Marion and V. Vié. 2007. Galactosyl headgroup interactions control the molecular packing of wheat lipids in Langmuir films and in hydrated liquid-crystalline mesophases. Biochimica et Biophysica Acta (BBA) - Biomembranes. 1768:1526-1540.

Caupin, F., A. Arvengas, K. Davitt, M.E.M. Azouzi, K.I. Shmulovich, C. Ramboz, D.A. Sessoms and A.D. Stroock. 2012. Exploring water and other liquids at negative pressure. Journal of Physics: Condensed Matter. 24:284110.

Caupin, F., M.W. Cole, S. Balibar and J. Treiner. 2008. Absolute limit for the capillary rise of a fluid. EPL. 82:1-6.

Chen, I.T., D.A. Sessoms, Z.M. Sherman, E. Choi, O. Vincent and A.D. Stroock. 2016. Stability limit of water by metastable vapor-liquid equilibrium with nanoporous silicon membranes. The Journal of Physical Chemistry B. 120:5209-5222.

Choat, B., M. Ball, J. Luly and J. Holtum. 2003. Pit membrane porosity and water stress-induced cavitation in four co-existing dry rainforest tree species. Plant Physiology. 131:41–48.

Choat, B., S. Jansen, T.J. Brodribb, H. Cochard, S. Delzon, R. Bhaskar, S.J. Bucci, T.S. Feild, S.M. Gleason, U.G. Hacke, A.L. Jacobsen, F. Lens, H. Maherali, J. Martinez-Vilalta, S. Mayr, M. Mencuccini, P.J. Mitchell, A. Nardini, J. Pittermann, R.B. Pratt, J.S. Sperry, M. Westoby, I.J. Wright and A.E. Zanne. 2012. Global convergence in the vulnerability of forests to drought. Nature. 491:752-755.

Christensen-Dalsgaard, K.K., M.T. Tyree and P.G. Mussone. 2011. Surface tension phenomena in the xylem sap of three diffuse porous temperate tree species. Tree Physiology. 31:361-368.

513 Cochard, H., T. Hölttä, S. Herbette, S. Delzon and M. Mencuccini. 2009. New insights into the
514 mechanisms of water-stress-induced cavitation in conifers. Plant Physiology. 151:949-
515 954.
516 Dixon, H.H. 1914a. On the tensile strength of sap. Scientific Proceedings of the Royal Dublin
517 Society. NS 14:229-234.
518 Dixon, H.H. 1914b. Transpiration and the ascent of sap in plants. Macmillan and Co., London,
519 UK. 216 p.
520 Dixon, H.H. and J. Joly. 1895. On the ascent of sap. Philosophical Transactions of the Royal
521 Society of London, Series B. 186:563-576.
522 Domec, J.C. 2011. Let's not forget the critical role of surface tension in xylem water relations.
523 Tree Physiology. 31:359-360.
524 Dörmann, P. and C. Benning. 2002. Galactolipids rule in seed plants. Trends in Plant Science.
525 7:112-118.
526 Duan, C., R. Karnik, M.-C. Lu and A. Majumdar. 2012. Evaporation-induced cavitation in
527 nanofluidic channels. Proceedings of the National Academy of Sciences. 109:3688-3693.
528 Esau, K. 1965. Plant anatomy, 2nd Edn. John Wiley & Sons, New York.
529 Esau, K., V.I. Cheadle and R.H. Gill. 1966. Cytology of differentiating tracheary elements. II.
530 Structures associated with cell surfaces. American Journal of Botany. 53:765-771.
531 Gibbs, J.W. 1906. The scientific papers. Vol. I. Thermodynamics. Longmans, Greens and Co.,
532 London. 434 p.
533 Gonorazky, G., A.M. Laxalt, H.L. Dekker, M. Rep, T. Munnik, C. Testerink and L. de la Canal.
534 2012. Phosphatidylinositol 4-phosphate is associated to extracellular lipoproteic fractions
535 and is detected in tomato apoplastic fluids. Plant Biology. 14:41-49.
536 Graham, R.C., P.J. Schoeneberger, M.A. Anderson, P.D. Sternberg and K.R. Tice. 1997.
537 Morphology, porosity, and hydraulic conductivity of weathered granitic bedrock and
538 overlying soils. Soil Science Society of America Journal. 61:516-522.

539 Gzyl-Malcher, B., M. Filek and K. Makyła. 2008. Langmuir monolayers of chloroplast
540 membrane lipids. Thin Solid Films. 516:8844-8847.
541 Hacke, U.G. and J.S. Sperry. 2001. Functional and ecological xylem anatomy. Perspectives in
542 Plant Ecology Evolution and Systematics. 4:97-115.
543 Hacke, U.G., J.S. Sperry, J.K. Wheeler and L. Castro. 2006. Scaling of angiosperm xylem
544 structure with safety and efficiency. Tree Physiology. 26:689-701.
545 Hemmingsen, E.A. 1978. Effects of surfactants and electrolytes on the nucleation of bubbles in
546 gas-supersaturated solutions. Zeitschrift für Naturforschung. 33a:164-171.
547 Hölttä, T., H. Cochard, E. Nikinmaa and M. Mencuccini. 2009. Capacitive effect of cavitation in
548 xylem conduits: results from a dynamic model. Plant Cell and Environment. 32:10-21.
549 Hölttä, T., E. Juurola, L. Lindfors and A. Porcar-Castell. 2012. Cavitation induced by a
550 surfactant leads to a transient release of water stress and subsequent 'run away' embolism
551 in Scots pine (*Pinus sylvestris*) seedlings. Journal of Experimental Botany. 63:1057-1067.
552 Hoyo, J., E. Guaus and J. Torrent-Burgués. 2016. Monogalactosyldiacylglycerol and
553 digalactosyldiacylglycerol role, physical states, applications and biomimetic monolayer
554 films. The European Physical Journal E. 39:39.
555 Ingenito, E.P., L. Mark, J. Morris, F.F. Espinosa, R.D. Kamm and M. Johnson. 1999.
556 Biophysical characterization and modeling of lung surfactant components. Journal of
557 Applied Physiology. 86:1702-1714.
558 Jansen, S., M. Klepsch, S. Li, M.M. Kotowska, S. Schiele, Y. Zhang and H.J. Schenk. 2018.
559 Challenges in understanding air-seeding in angiosperm xylem. Acta Horticulturae.
560 1222:13-20.
561 Jansen, S. and H.J. Schenk. 2015. On the ascent of sap in the presence of bubbles. American
562 Journal of Botany. 102:1561-1563.
563 Kaack, L., C.M. Altaner, C. Carmesin, A. Diaz, M. Holler, C. Kranz, G. Neusser, M. Odstrcil,
564 H.J. Schenk, V. Schmidt, M. Weber, Y. Zhang and S. Jansen. 2019. Function and three

565 dimensional structure of intervessel pit membranes in angiosperms: a review. IAWA
566 Journal. in press
567 Kalisch, B., P. Dörmann and G. Hölzl. 2016. DGDG and glycolipids in plants and algae. *In*
568 Lipids in plant and algae development Eds. Y. Nakamura and Y. L-Beisson. Springer,
569 Cham, Switzerland, pp 51-83.
570 Kanduč, M., A. Schlaich, A.H. de Vries, J. Jouhet, E. Maréchal, B. Demé, R.R. Netz and E.
571 Schneck. 2017. Tight cohesion between glycolipid membranes results from balanced
572 water–headgroup interactions. Nature Communications. 8:14899.
573 Kooijman, E.E., V. Chupin, B. de Kruijff and K.N. Burger. 2003. Modulation of membrane
574 curvature by phosphatidic acid and lysophosphatidic acid. Traffic. 4:162-74.
575 Kwan, J.J. and M.A. Borden. 2010. Microbubble dissolution in a multigas environment.
576 Langmuir. 26:6542-6548.
577 Lee, A.G. 2000. Membrane lipids: It's only a phase. Current Biology. 10:R377-R380.
578 Losso, A., B. Beikircher, B. Dämon, S. Kikuta, P. Schmid and S. Mayr. 2017. Xylem sap surface
579 tension may be crucial for hydraulic safety. Plant Physiology. 175:1135-1143.
580 Lucas, W.J., A. Groover, R. Lichtenberger, K. Furuta, S.R. Yadav, Y. Helariutta, X.Q. He, H.
581 Fukuda, J. Kang, S.M. Brady, J.W. Patrick, J. Sperry, A. Yoshida, A.F. Lopez-Millan,
582 M.A. Grusak and P. Kachroo. 2013. The plant vascular system: Evolution, development
583 and functions. Journal of Integrative Plant Biology. 55:294-388.
584 Marsh, D. and M.D. King. 1986. Prediction of the critical micelle concentrations of mono- and
585 di-acyl phospholipids. Chemistry and Physics of Lipids. 42:271-277.
586 Meinzer, F.C., D.R. Woodruff, D.E. Marias, D.D. Smith, K.A. McCulloh, A.R. Howard and A.L.
587 Magedman. 2016. Mapping 'hydroscapes' along the iso- to anisohydric continuum of
588 stomatal regulation of plant water status. Ecology Letters. 19:1343-1352.
589 Menzl, G., M.A. Gonzalez, P. Geiger, F. Caupin, J.L.F. Abascal, C. Valeriani and C. Dellago.
590 2016. Molecular mechanism for cavitation in water under tension. Proceedings of the
591 National Academy of Sciences. 113:13582-13587.

592 Meyra, A.G., V.A. Kuz and G.J. Zarragoicoechea. 2007. Geometrical and physicochemical
593 considerations of the pit membrane in relation to air seeding: the pit membrane as a
594 capillary valve. Tree Physiology. 27:1401-1405.
595 Nagle, J.F. and S. Tristram-Nagle. 2000. Structure of lipid bilayers. Biochimica et Biophysica
596 Acta (BBA)-Reviews on Biomembranes. 1469:159-195.
597 Oertli, J.J. 1971. The stability of water under tension in the xylem. Zeitschrift für
598 Pflanzenphysiologie. 65:195-209.
599 Or, D. and M. Tuller. 2002. Cavitation during desaturation of porous media under tension. Water
600 Resources Research. 38:19-1-19-14.
601 Parra, E. and J. Pérez-Gil. 2015. Composition, structure and mechanical properties define
602 performance of pulmonary surfactant membranes and films. Chemistry and Physics of
603 Lipids. 185:153-175.
604 Plavcová, L., S. Jansen, M. Klepsch and U.G. Hacke. 2013. Nobody's perfect: Can irregularities
605 in pit structure influence vulnerability to cavitation? Frontiers in Plant Science. 4:453.
606 Rice, O.K. 1926. Dynamic surface tension and the structure of surfaces. The Journal of Physical
607 Chemistry. 31:207-215.
608 Schenk, H.J., S. Espino, S.M. Rich-Cavazos and S. Jansen. 2018. From the sap's perspective: the
609 nature of vessel surfaces in angiosperm xylem. American Journal of Botany. 105:174-
610 187.
611 Schenk, H.J., S. Espino, D.M. Romo, N. Nima, A.Y.T. Do, J.M. Michaud, B. Papahadjopoulos-
612 Sternberg, J. Yang, Y. Zuo, K. Steppe and S. Jansen. 2017. Xylem surfactants introduce a
613 new element to the cohesion-tension theory. Plant Physiology. 173:1177-1196.
614 Schenk, H.J., S. Espino, A. Visser and B.K. Esser. 2016. Dissolved atmospheric gas in xylem sap
615 measured with membrane inlet mass spectrometry. Plant, Cell & Environment. 39:944-
616 950.

617 Schenk, H.J., J.M. Michaud, S. Espino, T. Melendres, M.R. Roth, R. Welti, L. Kaack and S.
618 Jansen. 2019. Lipids in xylem sap of woody plants across the angiosperm phylogeny.
619 bioRxiv:763771.
620 Schenk, H.J., K. Steppe and S. Jansen. 2015. Nanobubbles: a new paradigm for air-seeding in
621 xylem. Trends in Plant Science. 20:199-205.
622 Schürch, D., O.L. Ospina, A. Cruz and J. Pérez-Gil. 2010. Combined and independent action of
623 proteins SP-B and SP-C in the surface behavior and mechanical stability of pulmonary
624 surfactant films. Biophysical Journal. 99:3290-3299.
625 Simidjiev, I., S. Stoylova, H. Amenitsch, T. Jávorfi, L. Mustárdy, P. Laggner, A. Holzenburg and
626 G. Garab. 2000. Self-assembly of large, ordered lamellae from non-bilayer lipids and
627 integral membrane proteins *in vitro*. Proceedings of the National Academy of Sciences.
628 97:1473-1476.
629 Sperry, J.S. and M.T. Tyree. 1988. Mechanism of water stress-induced xylem embolism. Plant
630 Physiology. 88:581-587.
631 Stroock, A.D., V.V. Pagay, M.A. Zwieniecki and N.M. Holbrook. 2014. The physicochemical
632 hydrodynamics of vascular plants. *In* Annual Review of Fluid Mechanics, Vol 46 Eds.
633 S.H. Davis and P. Moin, pp 615-642.
634 Thut, H.F. 1928. Demonstration of the lifting power of evaporation. The Ohio Journal of
635 Science. 28:292-298.
636 Tyree, M.T. and M.H. Zimmermann. 2002. Xylem structure and the ascent of sap. Springer
637 Series in Wood Science, 2nd Edn. Springer-Verlag, Berlin. 283 p.
638 Valle, R.P., T. Wu and Y.Y. Zuo. 2015. Biophysical influence of airborne carbon nanomaterials
639 on natural pulmonary surfactant. ACS Nano. 9:5413-5421.
640 Vincent, O., P. Marmottant, P.A. Quinto-Su and C.-D. Ohl. 2012. Birth and growth of cavitation
641 bubbles within water under tension confined in a simple synthetic tree. Physical Review
642 Letters. 108:184502.

643 Wheeler, J.K., J.S. Sperry, U.G. Hacke and N. Huang. 2005. Inter-vessel pitting and cavitation in
644 woody Rosaceae and other vesseled plants: a basis for a safety vs. efficiency trade-off in
645 xylem transport. Plant, Cell and Environment. 28:800-812.
646 Wheeler, T.D. and A.D. Stroock. 2008. The transpiration of water at negative pressures in a
647 synthetic tree. Nature. 455:208-212.
648 Wheeler, T.D. and A.D. Stroock. 2009. Stability limit of liquid water in metastable equilibrium
649 with subsaturated vapors. Langmuir. 25:7609-7622.
650 Yang, J., K. Yu and Y.Y. Zuo. 2017. Accuracy of axisymmetric drop shape analysis in
651 determining surface and interfacial tensions. Langmuir. 33:8914-8923.
652 Yang, Y., L. Xu, S. Dekkers, L.G. Zhang, F.R. Cassee and Y.Y. Zuo. 2018. Aggregation state of
653 metal-based nanomaterials at the pulmonary surfactant film determines biophysical
654 inhibition. Environmental Science & Technology. 52:8920-8929.
655 Yount, D.E. 1979. Skins of varying permeability: A stabilization mechanism for gas cavitation
656 nuclei. Journal of the Acoustical Society of America. 65:1429-1439.
657 Yount, D.E. 1997. On the elastic properties of the interfaces that stabilize gas cavitation nuclei.
658 Journal of Colloid and Interface Science. 193:50-59.
659 Yount, D.E., T.D. Kunkle, J.S. D'Arrigo, F.W. Ingle, C.M. Yeung and E.L. Beckman. 1977.
660 Stabilization of gas cavitation nuclei by surface-active compounds. Aviation, Space, and
661 Environmental Medicine. 48:185-191.
662 Zhang, Y., C. Carmesin, L. Kaack, M.M. Klepsch, M. Kotowska, T. Matei, H.J. Schenk, M.
663 Weber, P. Walther, V. Schmidt and S. Jansen. 2019. High porosity with tiny pore
664 constrictions and unbending pathways characterise the 3D structure of intervessel pit
665 membranes in angiosperm xylem. Plant, Cell and Environment. in press
666 Zhang, Y., M. Klepsch and S. Jansen. 2017. Bordered pits in xylem of vesselless angiosperms
667 and their possible misinterpretation as perforation plates. Plant, Cell & Environment.
668 40:2133-2146.

669 Zimmermann, M.H. 1983. Xylem structure and the ascent of sap. Springer Series in Wood
670 Science. Springer-Verlag, Berlin. 143 p.
671 Zuo, Y.Y., R.A. Veldhuizen, A.W. Neumann, N.O. Petersen and F. Possmayer. 2008. Current
672 perspectives in pulmonary surfactant--inhibition, enhancement and evaluation.
673 Biochimica et Biophysica Acta. 1778:1947-1977.

674

675

Table 1. Composition of xylem sap lipids (in % of molar composition) for the four studied species determined by direct-infusion electrospray ionization triple-quadrupole mass spectrometry, arranged by headgroups and expressed as mean ± standard error percentage of total lipids (Schenk et al. 2019). Acyl chains (not shown here) most commonly had 34 or 36 carbon atoms, and >98% of acyl chains were unsaturated, mostly featuring 1-3 double bonds for 34 carbon atom acyl chains and 3-5 double-bonds for 36 carbon atom acyl chains (Schenk et al. 2019).

Percent of all lipids	*Liriodendron tulipifera*	*Geijera parviflora*	*Distictis buccinatoria*	*Encelia farinosa*
Galactolipids				
DGDG	7.8 ± 3.1	3.3 ± 0.7	9.1 ± 1.3	2.9 ± 0.9
MGDG	26.6 ± 12.6	7.1 ± 1.5	11.0 ± 2.1	4.0 ± 1.1
Phospholipids				
PA	21.7 ± 9.3	48.9 ± 15.8	33.9 ± 11.5	49.6 ± 15.8
PC	21.2 ± 5.3	15.3 ± 3.9	19.3 ± 4.1	13.5 ± 5.8
PE	8.4 ± 4.2	11.1 ± 2.1	10.2 ± 2.3	8.7 ± 6.0
PI	4.8 ± 2.9	7.8 ± 3.5	11.3 ± 3.8	13.4 ± 8.8
PS	2.3 ± 1.1	3.4 ± 0.8	2.9 ± 1.1	2.8 ± 1.6
PG	1.2 ± 0.5	0.7 ± 0.4	0.6 ± 0.2	0.8 ± 0.5
LysoPG	4.4 ± 0.8	1.8 ± 0.8	1.2 ± 0.3	1.9 ± 0.3
LysoPC	1.5 ± 1.0	0.3 ± 0.1	0.2 ± 0.1	1.4 ± 0.4
LysoPE	0.3 ± 0.2	0.2 ± 0.1	0.2 ± 0.1	0.9 ± 0.5

Galactolipids: DGDG = digalactosyldiacylglycerol, MGDG = and monogalactosyldiacylglycerol. Phospholipids: PA = phosphatidic acid, PC = phosphatidylcholine, PE = phosphatidylethanolamine, PI = phosphatidylinositol, PS = phosphatidylserine, PG = phosphatidylglycerol, LysoPG = lysophosphatidylglycerol, LysoPC = lysophosphatidylcholine, LysoPE = lysophosphatidylethanolamine.

Figures

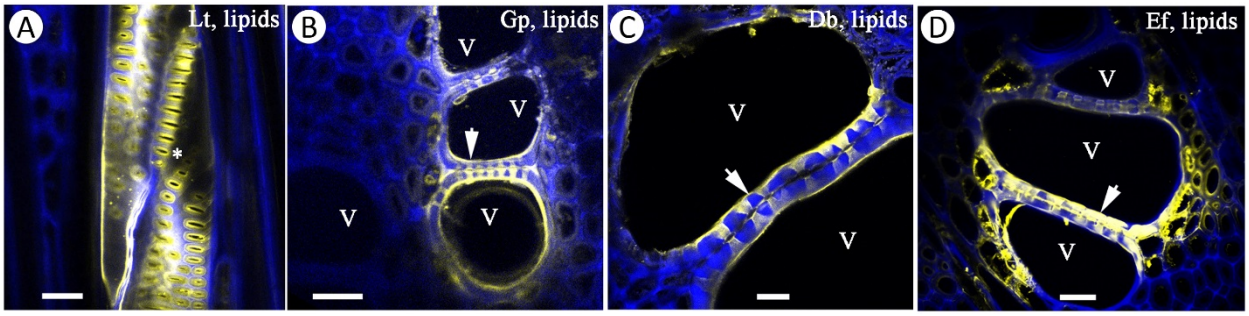

Figure 1. Confocal microscopy images of transverse and tangential cell walls in secondary xylem after vacuum infiltration with FM®1-43 fluorophores (yellow color) to detect amphiphilic lipids; in vessel walls and bordered intervessel pits. Image A is a longitudinal view, while all other images are transverse views. Because the secondary xylem area scanned was some distance below the injection point, the fluorophores do not occur in all conduits. Blue colored walls show lignin autofluorescence. Lt = *Liriodendron tulipifera*, Gp = *Geijera parviflora*, Db = *Distictis buccinatoria*, Ef = *Encelia farinosa*, V = vessel, short arrows = intervessel walls with intervessel pits. All scale bars represent 20 µm. Reproduced and slightly modified from Schenk et al. (2018) with permission.

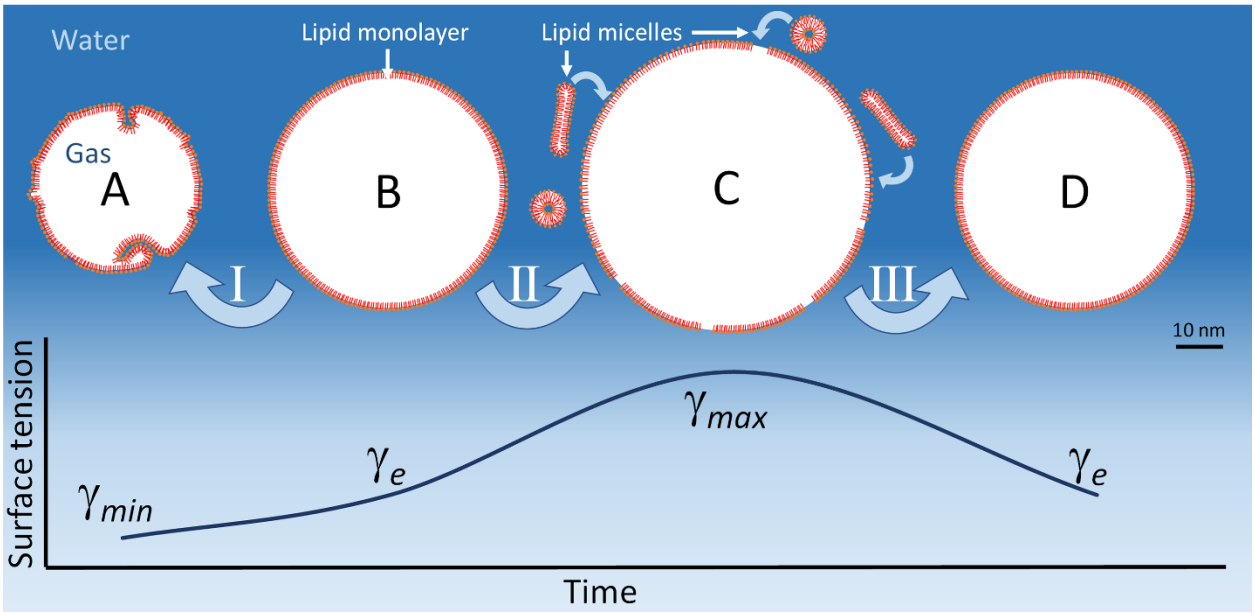

689 Figure 2. Conceptual illustration of dynamic surface tension shown for the example of amphiphilic
690 lipid films on gas bubbles in water, depending both on surface area and time. Sizes of lipid
691 molecules and bubbles are roughly to scale. A = collapsed lipid film, showing both outward- and
692 inward folding of the lipid layer; B = lipid monolayer at equilibrium surface tension; C = bubble
693 expansion leading to stretched monolayer with dense and stretched lipid domains and some gaps,
694 which can potentially be filled in by the adjacent lipid micelles, if they are present and given
695 enough time; D = bubble compression leading back to equilibrium surface tension. I =
696 compression, II = expansion, III = compression. Note that bubbles A-D are each coated by the
697 same number of lipid molecules.
698
699

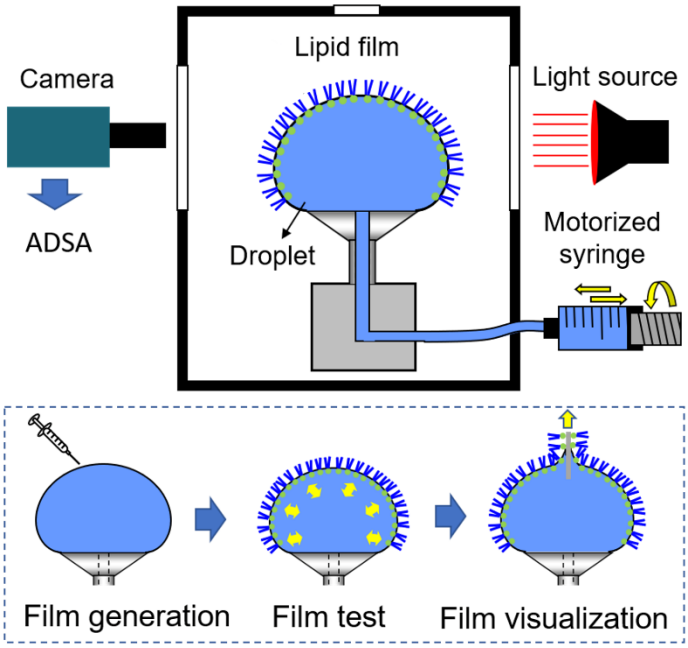

Figure 3. Schematic of the constrained drop surfactometry (CDS) for studying the surface activity of lipid films. A liquid droplet is "constrained" on a 3−5 mm carefully machined pedestal with a knife-sharp edge. The lipid film can be periodically compressed and expanded by precisely regulating liquid flow into and out of the droplet with a motorized syringe. The surface tension and surface area of the lipid film are simultaneously determined from the shape of the droplet using axisymmetric drop shape analysis. ADSA = axisymmetric drop shape analysis; Dynamic ST = dynamic surface tension; LB transfer = transfer of lipids to create a Langmuir-Blodgett film for atomic force microscopy.

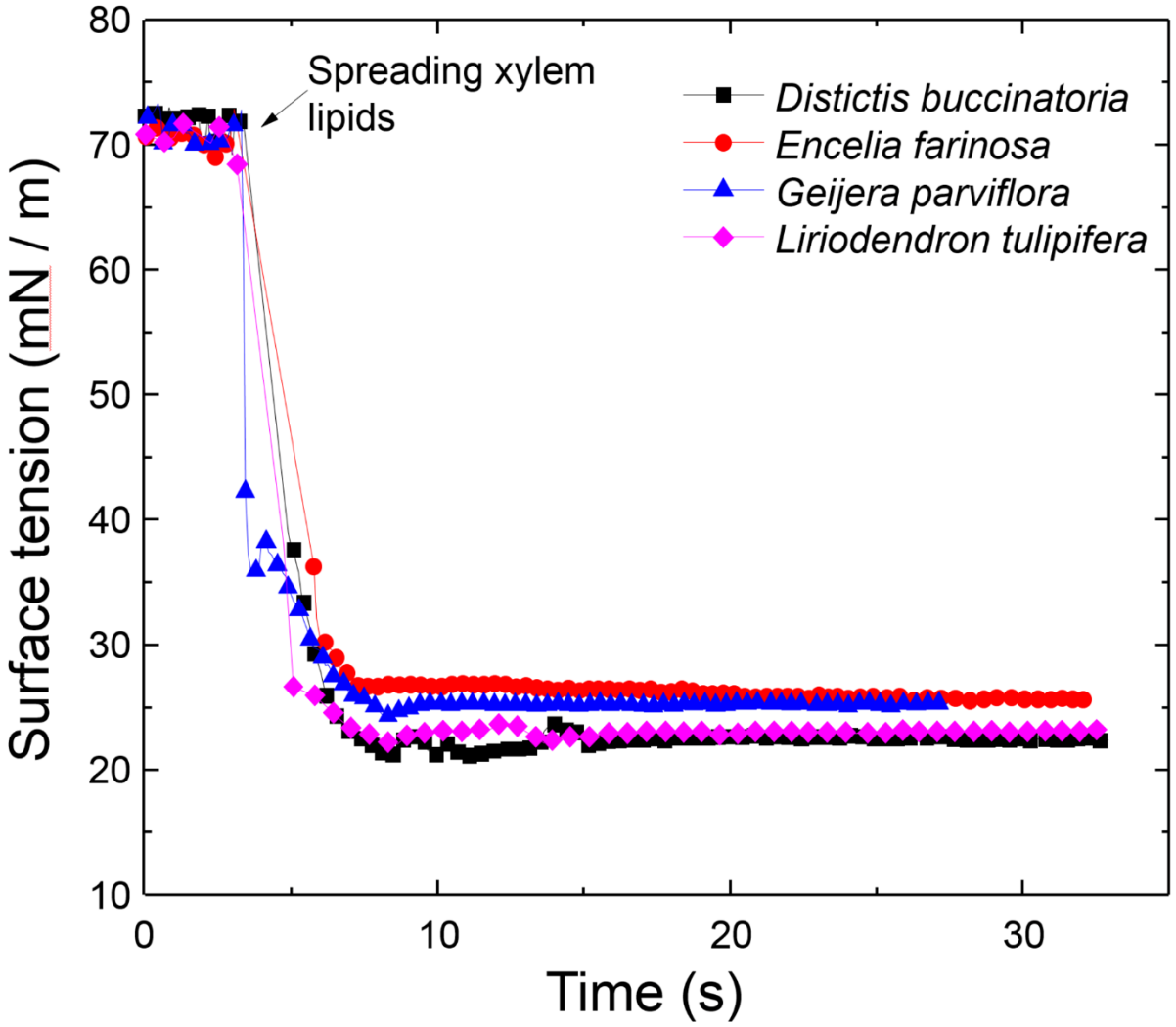

710 Figure 4. Time-dependent dynamic surface tension of natural xylem lipids from four woody
711 angiosperm species, measured via CDS and axisymmetric drop shape analysis (Figure 3) starting
712 with a pure water droplet at time zero (72 mN / m) and after adding xylem lipids to the droplet at
713 about 3 seconds, leading to an immediate drop in surface tension to around 37 mN / m and then
714 reaching equilibrium surface tension, γ_e, around 25 mN / m within a few seconds.

715
716

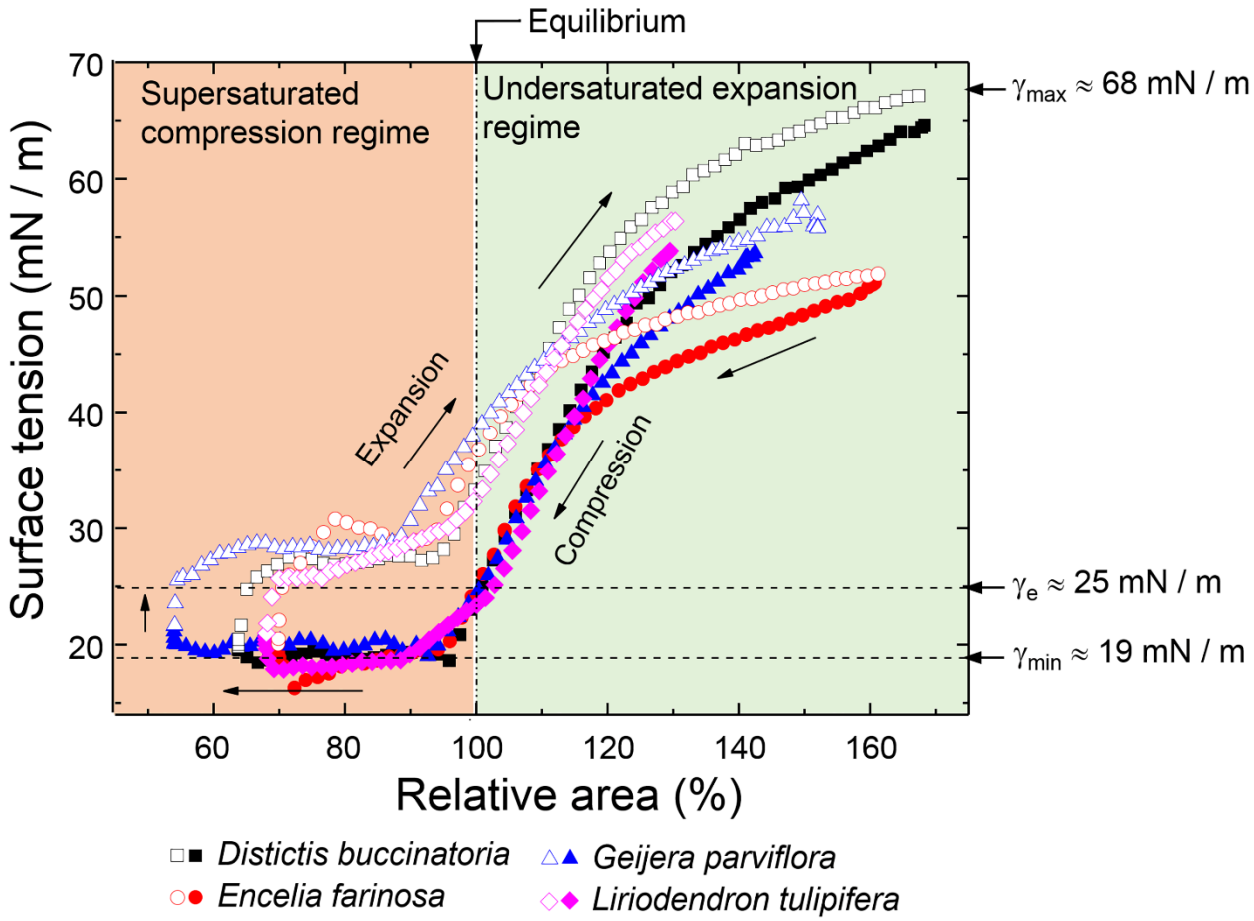

717 Figure 5. Surface area-regulated surface tension of xylem lipids from four woody angiosperm
718 species. Film compression is indicated by solid symbols and film expansion is indicated by open
719 symbols. Lipids from all four species show similar compression and expansion cycles. Cycles start
720 at 100% relative surface area, followed by compression to 50-70% and expansion to 140-170% of
721 surface area. Explanation of symbols: γ_{max} = maximum surface tension on expanded surface area,
722 γ_e = equilibrium surface tension at 100% relative surface area, γ_{min} = minimum surface tension of
723 collapsed lipid layers.

724
725

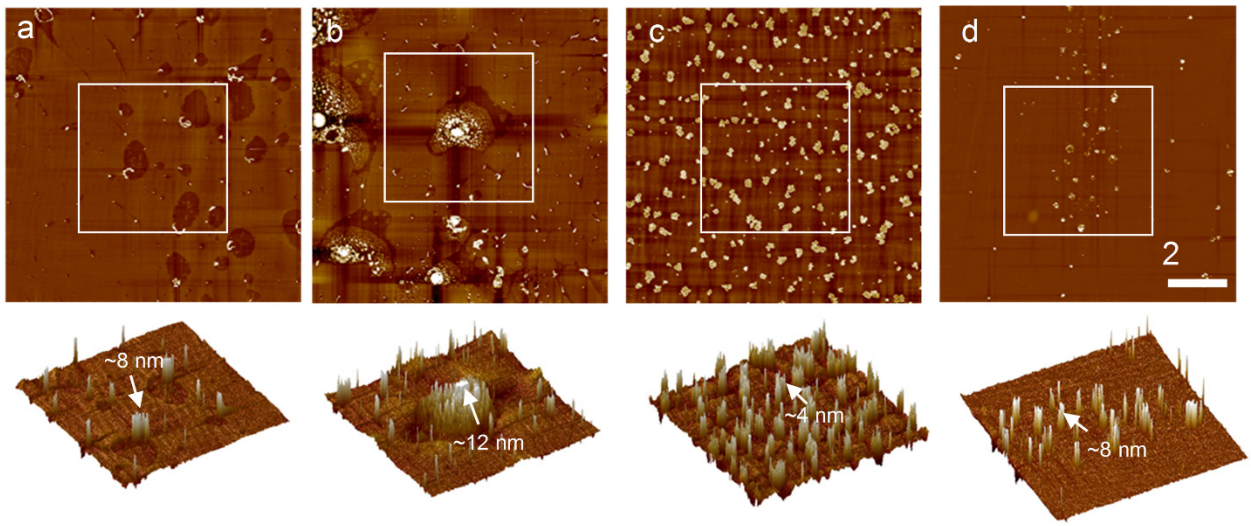

726 Figure 6. AFM topographic images of four natural xylem lipid films close to equilibrium surface
727 tension (see Figure 5). The films were created by moving a clean mica sheet through a lipid film
728 at equilibrium. a. *Distictis buccinatoria*, b. *Encelia farinosa*; c. *Geijera parviflora*, and d.
729 *Liriodendron tulipifera*. AFM images in the first row have the same scanning area of 10×10 μm
730 and the *z*-range of 20 nm. Images in the second row show the surface render of the zoom-in xylem
731 surfactant film as indicated by the white boxes. White arrows indicate the heights of the
732 multilayered structures.
733

Supporting information

Dynamic Surface Tension of Xylem Sap Lipids

Jinlong Yang[1], Joseph Michaud[2], Steven Jansen[3], H. Jochen Schenk[2], and Yi Y. Zuo[1,4*]*

1. Department of Mechanical Engineering, University of Hawaii at Manoa, Honolulu, Hawaii, 96822, USA
2. Department of Biological Science, California State University, Fullerton, California 92831, USA
3. Institute of Systematic Botany and Ecology, Ulm University, Albert-Einstein-Allee 11, D–89081, Ulm, Germany
4. Department of Pediatrics, John A. Burns School of Medicine, University of Hawaii, Honolulu, Hawaii, 96826, USA

***Corresponding authors:**

Email: jschenk@fullerton.edu (H. Jochen Schenk)

E-mail: yzuo@hawaii.edu (Yi Y. Zuo)

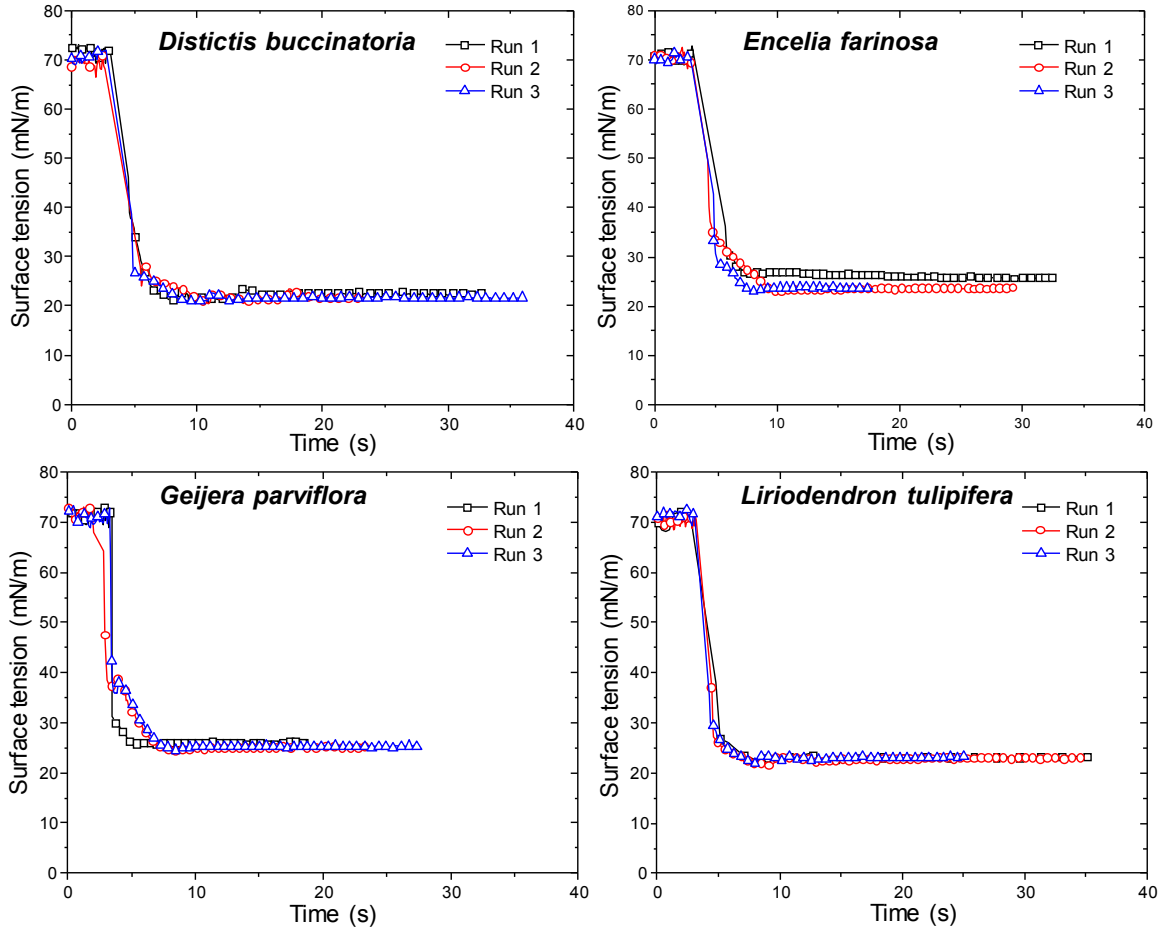

Figure S1. Reproducibility of the dynamic surface tensions of xylem lipids from four woody angiosperm species.

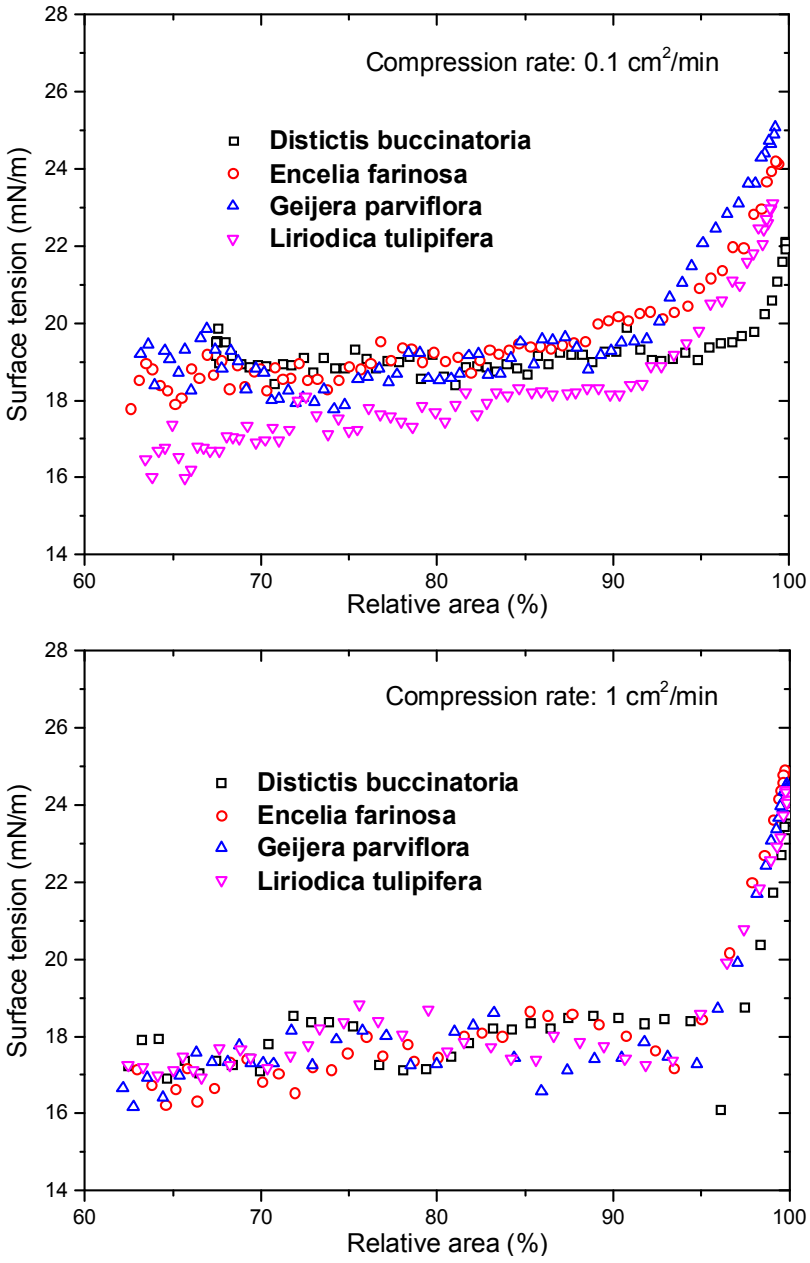

Figure S2. Compression of the film with two compression rates: 0.1 cm^2/min and 1 cm^2/min. Given the lack of differences between compression rates, different expansion rates are not shown.

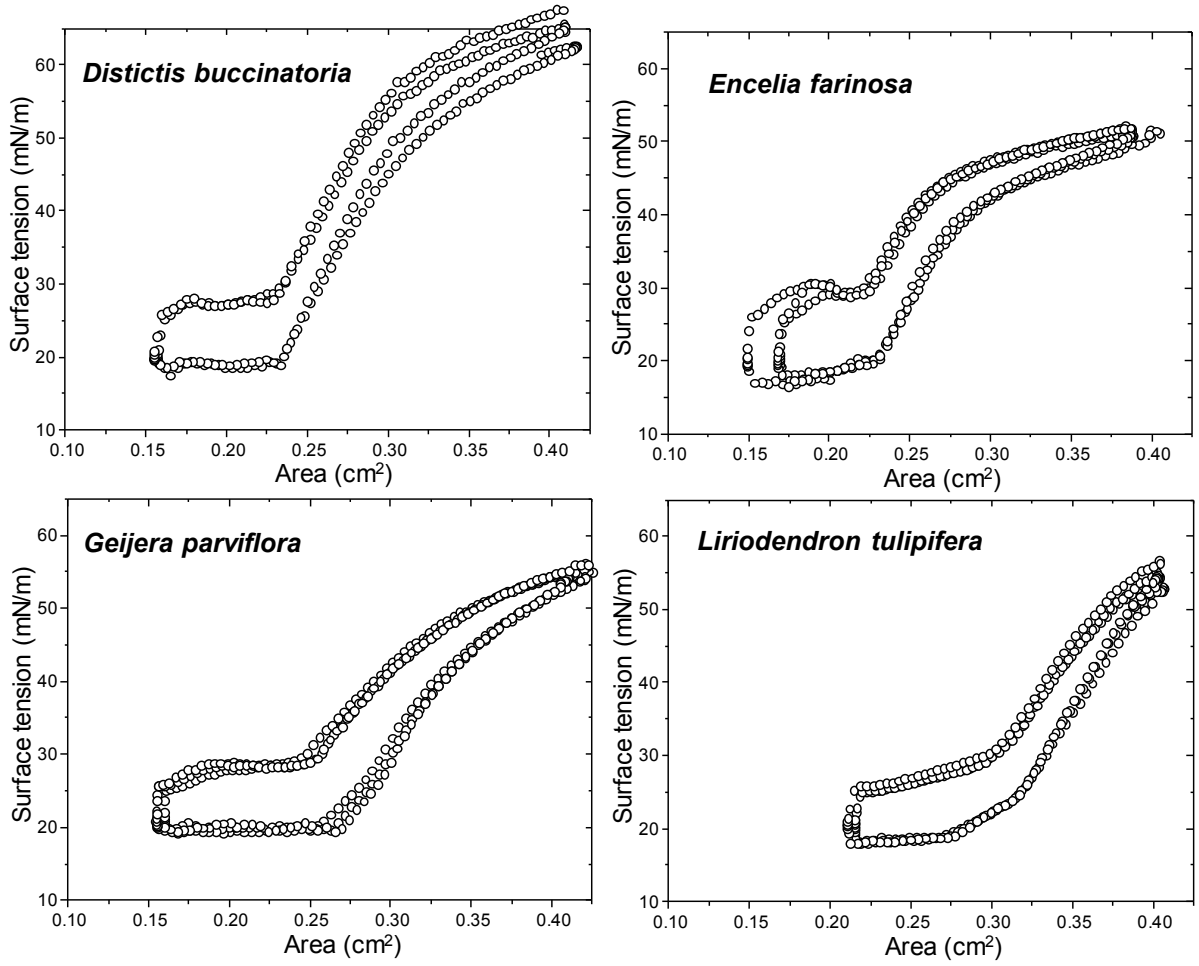

Figure S3. Reproducibility of the surface area-regulated surface tensions of xylem lipids from four woody angiosperm species.

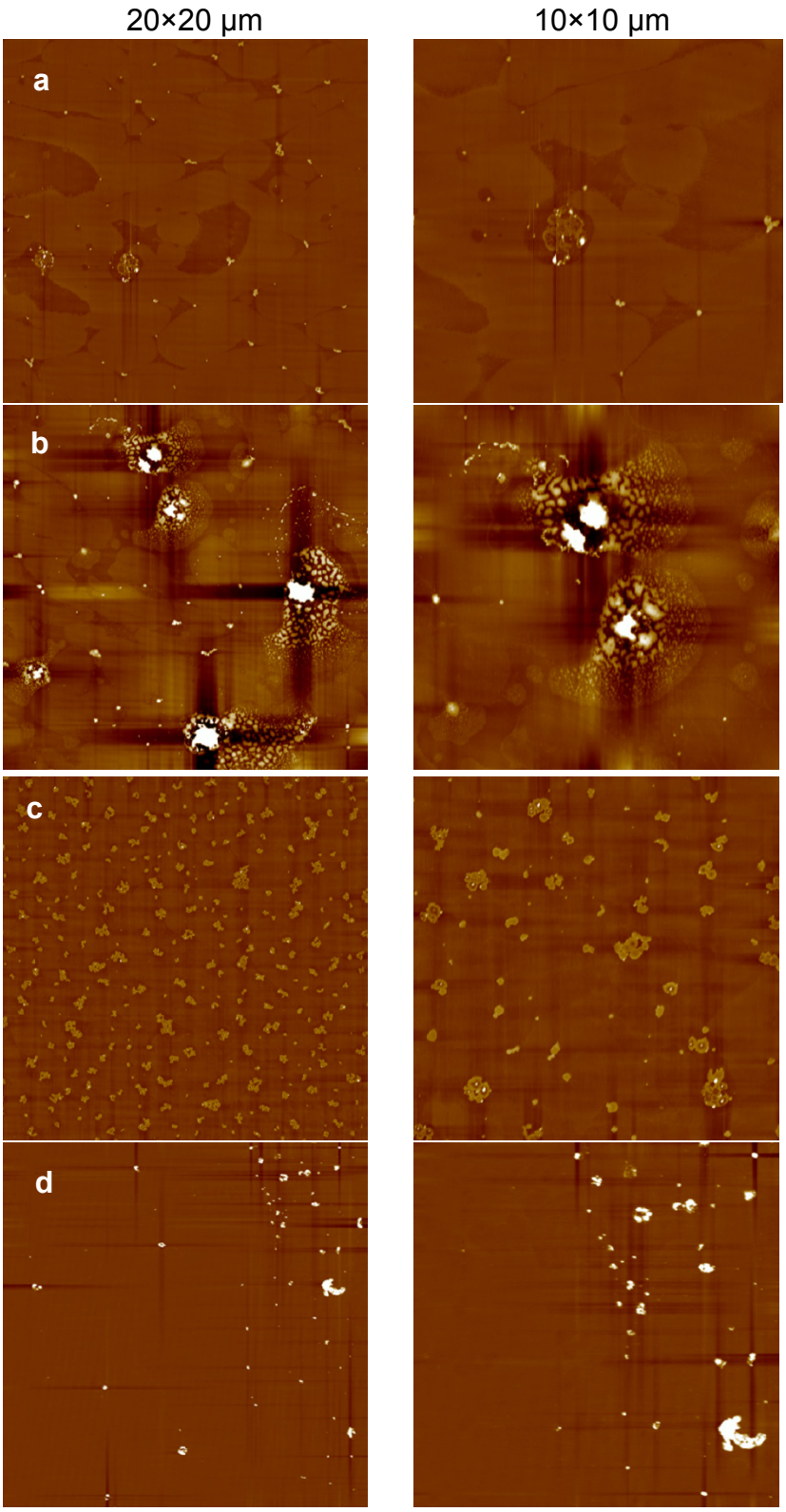

Figure S4. Reproducibility of atomic force microscopy (AFM) topographic images of xylem lipids from four woody angiosperm species. a. *Distictis buccinatoria*, b. *Encelia farinosa*; c. *Geijera parviflora*, and d. *Liriodendron tulipifera*. AFM images in the first and second columns have the scanning area of 20×20 µm and 10×10 µm, respectively.